

# Weaving Off-The-Shelf Yarns into Textile Micro Total Analysis Systems ( $\mu$ TAS)

Ingrid Öberg Månsson, Andrew Piper,\* and Mahiar Max Hamedi\*

Textile based biosensors have garnered much interest in recent years. Devices woven out of yarns have the ability to be incorporated into clothing and bandages. Most woven devices reported in the literature require yarns that are not available on an industrial scale or that require modifications which are not possible in large scale manufacturing. In this work, commercially produced yarns are taken without any modification or cleaning, and developed woven textile diagnostic devices out of them. The yarn properties that are important to their function within the device have been characterised and discussed. The wicking ability and analyte retention of Coolmax yarns, developed to wick sweat in mass produced sportswear, are determined. The electrochemistry and functionalizability of Au coated multifilament yarns are investigated with no cleaning or treatment and are found to have as good a thiolate self-assembled monolayer (SAM) coverage as cleaned Au disk electrodes. The feasibility of using these yarns is established off the shelf, with no cleaning, to make woven capillary force driven microfluidic devices and three electrode sensing devices. A proof of principle three electrode system capable of detecting clinically relevant concentrations of glucose in human sweat is reported.

The field of diagnostics has for many years now been pushing toward miniaturized point-of-care devices.<sup>[1–4]</sup> These have typically been made using microfabrication technologies.<sup>[5–8]</sup> However, these often require complex and expensive fabrication. An alternative approach has been the development of paper based diagnostics, a topic which has garnered much interest in recent years.<sup>[9–12]</sup> Another interesting alternative is to develop diagnostic platforms on textiles.<sup>[13,14]</sup> Not only does this approach, like paper, allow for the cheap creation of diagnostic devices, but textiles can easily and cheaply be woven or knit in a variety of patterns to introduce function on an industrial scale.<sup>[15]</sup> Unlike paper based devices textiles have the advantage of being wearable due to their stretch ability and wet stability. To this end, there has been some works focusing on the development

of smart bandages,<sup>[16]</sup> diagnostic diapers<sup>[14]</sup> and wearable sensors for sweat based diagnostics<sup>[17–19]</sup> on textile based platforms. Previous works by Reches et al.<sup>[20]</sup> have, for example, investigated the wicking properties of several threads for use in diagnostics as well as comparing methods of controlling the wicking within threads. As with other papers in the field the focus has been on the development of colorimetric tests,<sup>[20–22]</sup> chemical/pH tests<sup>[23]</sup> and immunoassay tests.<sup>[24]</sup> Electrochemical detection on textiles has been reported previously but usually requires the “in house” modification of commercial yarns in a manner that makes them less scalable or the focus on the novel fabrication of functional yarns.<sup>[25]</sup> For example, Liu and Lillehoj<sup>[26]</sup> have developed a three electrode electrochemical sensor by coating polyester threads with carbon and Ag/AgCl ink before stitching them into a fabric substrate. Glucose oxidase and lactate oxidase were adsorbed on the thread based working electrode by immersing the thread in solution to enable sensing of glucose and lactate in buffer and whole blood. Similarly, Choudhary et al.<sup>[27]</sup> have coated yarns in house to create the same type of electrodes which were then integrated in a woven device to realize sensing of glucose and hemoglobin in whole blood.

The ability to combine yarns with different properties using textile manufacturing processes to integrate function directly into the structure of the textile material is one of the key benefits of textile based diagnostics.<sup>[13–15]</sup> For analytical devices specifically, the bottom up fabrication of textiles allows us to use the micrometer scale dimension of yarns to achieve microelectronic or microfluidic structures without the need for microfabrication technologies.<sup>[13]</sup> Combining yarns with different properties such as electrical conductivity, wicking/nonwicking, or biofunctionalized yarns allows the fabrication of complete diagnostic tests entirely out of yarns using existing textile manufacturing technology.<sup>[13]</sup> There is a sparsity in the literature of works focusing on the characterization of commercially available yarns for electrochemical diagnostics. To that end, in this work we have characterized the properties of selected commercially available yarns that are suitable building blocks for diagnostics. One of the major advantages of this work is that the yarns are used as they arrive without the need for further processing which makes them suited for large scale manufacturing. We compare the wicking properties of Coolmax yarns and conductive properties of Au, Ag, and CNT coated

tate oxidase were adsorbed on the thread based working electrode by immersing the thread in solution to enable sensing of glucose and lactate in buffer and whole blood. Similarly, Choudhary et al.<sup>[27]</sup> have coated yarns in house to create the same type of electrodes which were then integrated in a woven device to realize sensing of glucose and hemoglobin in whole blood.

I. Öberg Månsson, Dr. A. Piper, Dr. M. M. Hamedi  
Department of Fibre and Polymer technology  
KTH Royal Institute of Technology  
Teknikringen 56, Stockholm 10044, Sweden  
E-mail: piper2@kth.se; mahiar@kth.se

 The ORCID identification number(s) for the author(s) of this article can be found under <https://doi.org/10.1002/mabi.202000150>.

© 2020 The Authors. Published by WILEY-VCH Verlag GmbH & Co. KGaA, Weinheim. This is an open access article under the terms of the Creative Commons Attribution License, which permits use, distribution and reproduction in any medium, provided the original work is properly cited.

DOI: 10.1002/mabi.202000150



yarns that are commercially available on a large scale. The suitability of these yarns for diagnostics is considered throughout and their ability to be woven into simple capillary force driven microfluidic devices is demonstrated. As a final proof of concept, devices are made using the most appropriate yarns that are capable of detecting glucose in artificial human sweat over the clinically relevant range.

The yarns used in this study can be broadly characterized by their function; there are the nonconductive yarns that are used for fluid transport, the conductive yarns used for electrochemical sensing and the monofilament yarn used as a barrier network to isolate fluid transport. The basic structure and properties of these yarns that are relevant to their incorporation in textile based diagnostic devices are provided in Table S1 (Supporting Information) and a photo of all yarns used is provided in Figure S3A (Supporting Information). It makes logical sense to begin by discussing the basic structures of the yarns, as many of their properties are derived from their structures. We will start by discussing the structure of the nonconductive yarns, as seen in Figure S4 (Supporting Information). The yarns chosen for fluidic transport are polyethylene terephthalate (PET) multifilament yarns that have been extruded to have microfluidic capillaries running down the length of the filaments through which they wick by capillary action. A more in-depth discussion of the structures of the yarns tested has been included in Section S1 (Supporting Information). Coolmax was chosen as a fluidic transport yarn in these studies as it has been designed for the sportswear industry with the specific intention of wicking sweat so it is an obvious choice as a fluid transport material. The monofilament is made of polyamide (Nylon) and used exclusively in this study because it does not wick so can be used as a fluidic separator in the woven structures. As can be seen in Table S1 (Supporting Information), all yarns have a corresponding yarn number. The different systems for yarn numbering are further explained elsewhere.<sup>[29]</sup>

All of the conductive yarns are composed of an inner core of multiple PET filaments that have been modified on an industrial scale to be conductive. The first of these is the Au yarn, in which each of the 72 individual filaments have been plasma coated with a nanometer thin layer of Au. SEM images of these yarns have been provided in Figures S3 and S5 (Supporting Information). The Ag yarn was purchased from the same supplier as the Au yarn (Swicofil) and has been produced in the same fashion by plasma coating the individual filaments. It is important to note at this point that because these are multifilament yarns both the Au and Ag yarns will wick fluids, driven by capillary forces between the filaments in their structure. The Ag yarn has been used as a pseudo-reference electrode in some of this work and was chosen as it is an ideal platform for future work where it can be converted into a formal Ag/AgCl reference electrode. The carbon nanotube (CNT) coated have been dip coated in a CNT paste. The structure of these CNT yarns, see Figure S5 in the Supporting Information, means that they do not wick by capillary forces between the filaments but the yarn does wick slowly through the paste.

To integrate capillary force driven microfluidic yarns in textile devices we first need to examine the wicking properties of the yarns. The different wicking yarns were vertically dipped into a solution of ultrapure water with methylene blue to

visualize the distance over which they wicked, see Figure S1 in the Supporting Information. The distance wicked versus time have been plotted in Figure 1A, showing that the dtex78/f48/2 and dtex78/f48/4 (both hexachannel) wicks faster and longer distances than the Ne 24/2 (tetrachannel). After 2 min, they have levelled off completely whereas the Ne 24/2 continues to wick during the whole test period. Further, we have plotted the distance versus square root of time, indicating that the fluid in the yarns flow according to the Washburn equation (Equation (1))

$$L = \sqrt{\left(\frac{\gamma r t \cos(\phi)}{2\eta}\right)} \quad (1)$$

where  $L$  is the wicked distance,  $\gamma$  is the surface tension,  $r$  is the pore radius,  $t$  is the time,  $\phi$  is the contact angle between the liquid and the yarn, and  $\eta$  is the dynamic viscosity of the liquid. When analyzing the wicking properties along a single yarn we can assume that  $\gamma$ ,  $r$ ,  $\phi$ , and  $\eta$  are all constant, therefore the distance is directly proportional to the square root of  $t$  which is shown in Figure 1B. Similar methods of wicking analysis for fluidic materials has previously been reported by several others.<sup>[24,30–33]</sup>

When comparing wicking between different Coolmax yarns, all the parameters in Equation (1) can be assumed to be constant except for  $r$ . This is a safe assumption to make since all the yarns are made from PET so their contact angle ( $\phi$ ) should be the same. Also they are all tested in a solution of water with the same concentration of dye so the values of  $\gamma$  and  $\eta$  are the same. Therefore, the difference in wicking between the yarns must be solely due to the difference in the average pore diameters between them. In the case of the tetrachannel Coolmax this is due to the structure on the micrometer scale having larger average channel diameters than the hexachannel yarns. When comparing the other two Coolmax yarns, the yarn with the greater number of filaments wicked farther and faster than the other. This is no doubt due to the increased average  $r$  caused by wicking through channels formed between filaments in the yarn. It is an important consideration that having more filaments in the yarn can increase the wicking rate and distance, but more filaments will also retain more of the analyte of interest because of their larger surface areas.

While the conductive yarns were all observed to wick (they would short at the connectors if nail varnish was not used to isolate the wetting area), they could not be tested by the same methods as the wicking yarns. Due to their color we could not determine the wicking rate or distance of the methylene blue dye on any of them. Given that they will not be used for fluid transport, all that matters is that they wet completely and quickly over the defined sensing area so that in the finished woven devices, see Figure 4, the measured electrochemical signal would be stable over time. To establish that this is the case, the yarns were imaged after analysis and PBS salt crystals could be seen at the ends of the conductive yarns, thereby proving that they had completely wet, Figure S6A (Supporting Information). CVs of the yarns over time have also been provided in Figure S6B to evidence the stability of the electrochemical response.

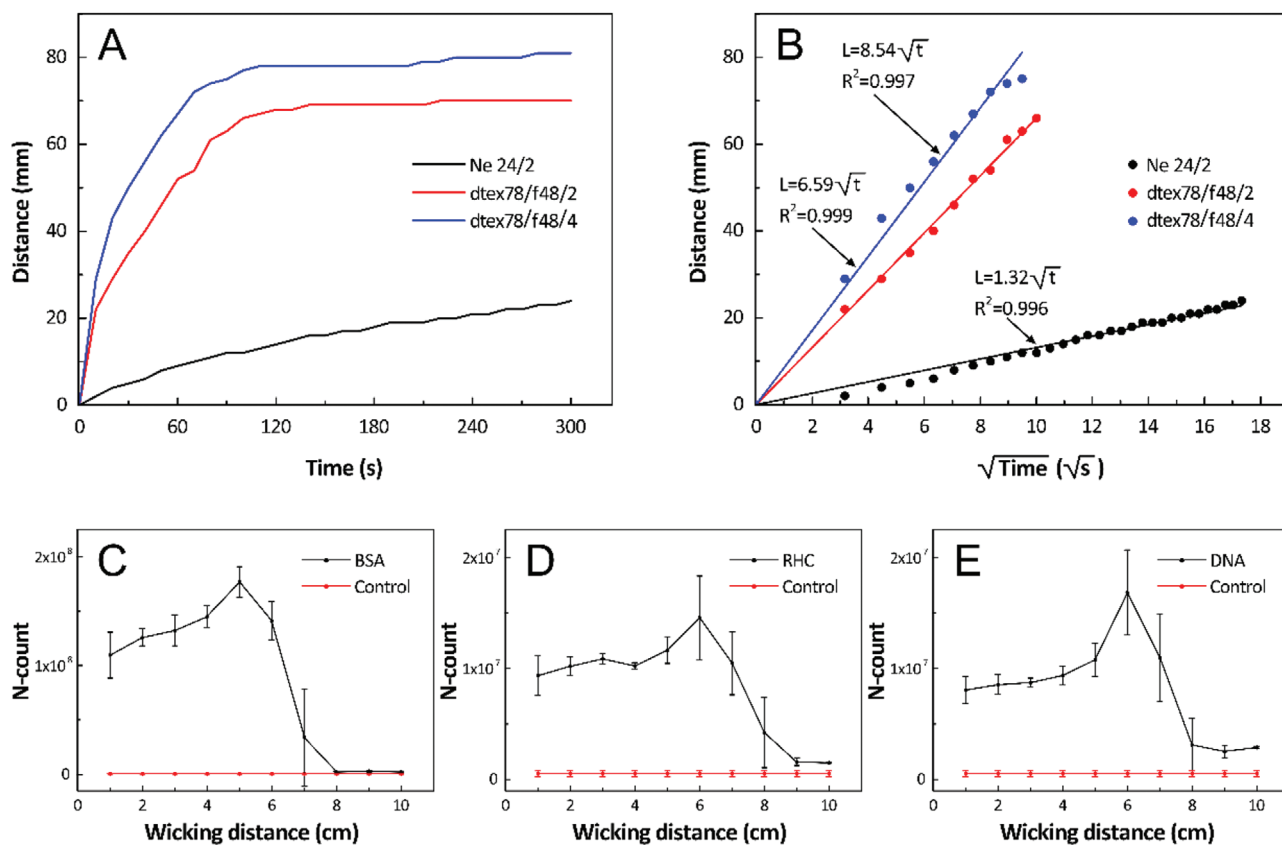


**Figure 1.** A) Wicking behavior, B) fit to Washburn equation, and C–E) concentration gradients over wicking distance. The control line shows nitrogen content for bare yarn cuts.

Another method of characterizing the fluidic yarns which is important to making diagnostic devices is to measure the loss of sample that is transported along the yarn. To do this we wicked 17 mer synthetic ssDNA, bovine serum albumin (BSA) and ruthenium hexamine chloride (RHC) as models for nucleic acid, protein and small molecules, respectively, across a yarn. These were all chosen as they contain nitrogen which could be analyzed in a nitrogen analyzer (ANTEK). After wicking and drying, each of the yarns were cut into 1 cm fragments and these were analyzed in turn to determine a concentration profile across the yarn for each of the model targets. The results of these tests for the Coolmax dtex78/f48/2 are provided in Figure 1C–E. In these results we can see that the three targets all wick to the same final distance and that there is not a constant loss of sample over distance. The concentration is roughly steady over the wicked distance but experiences a small spike at the end of where it has wicked. It is proposed that Marangoni effects are concentrating the target at the solvent front. This is an important consideration for sensing devices as when the sample solution first contacts the conductive element the concentration will be higher than that of the bulk sample. It is therefore advisable to introduce a wait time before making the first measurement and to design the device such that the sensing elements are within a region of the fluidic yarn where the target concentration is constant after initial wetting.

The conductive yarns were all initially characterized by measuring their resistance per centimeter, as seen in Table S1 (Supporting Information). The general trend between the Au, Ag, and CNT yarns is that the silver is the most conductive followed by the Au and then the CNT. This is in good agreement with the expected trend from the known resistivity's of these materials, it is also satisfying that the absolute values of these resistances per cm are in agreement with literature values.<sup>[34,35]</sup> As mention previously the Ag yarn was selected as a platform onto which formal Ag/AgCl reference electrodes could be developed. It is not common to use silver as a working electrode and as such it has only been used as a pseudoreference electrode in these studies. The Au and CNT yarns, however, were tested as working electrodes in a three electrode system. This was done in solutions of PBS with FC, RHC, or MB. First, the yarn working electrodes were tested against a commercial Pt counter electrode and Ag/AgCl reference electrode before these were consecutively swapped out with the Ag yarn as a pseudoreference and multiple Au yarns as a counter electrode. The resulting CVs have been provided in Figure 2. It should be reiterated that in all these tests the Au yarns were used as provided with no cleaning or conditioning steps. It is therefore pleasing that such nice voltammograms could be obtained, both in terms of their shape, peak current, and reproducibility. The peak separation in Figure 2A, for example, is  $55 \pm 6$  mV for the clean electrode, which increases to  $79 \pm 5$  mV when a MCH

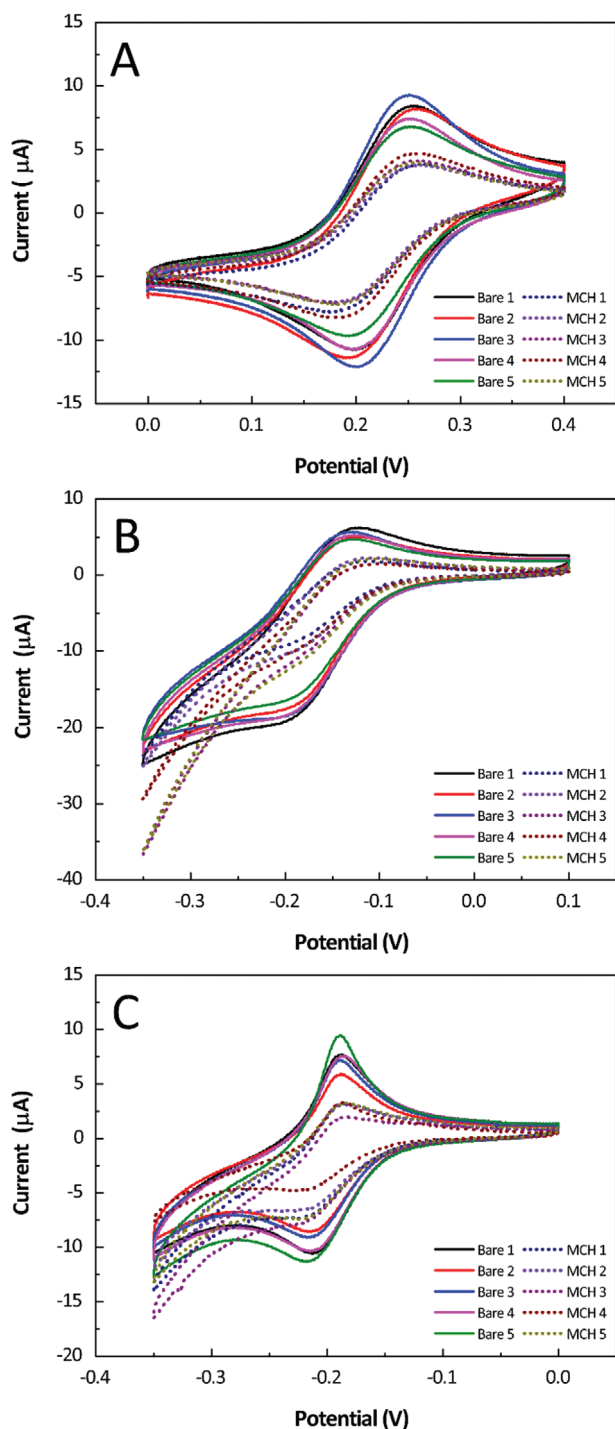


**Figure 2.** Au coated yarn as working electrode against standard Pt counter and Ag/AgCl reference electrode in A) potassium ferricyanide (FC), B) ruthenium hexamine chloride (RHC), and C) methylene blue (MB).

SAM is formed; which is the same as the theoretically lowest possible peak separation for a one electron transfer.<sup>[34]</sup>

The Au yarns were then functionalized overnight in ethanol with  $1 \times 10^{-3}$  M MCH before their CVs in each of the above buffers was remeasured, see dotted lines in Figure 2. By

measuring the peak current for the redox agent before and after self-assembled monolayer (SAM) formation we were able to assess the surface coverage of MCH as a model system for functionalization of the Au yarns. The five bare Au yarns cut and patterned to 13 mm long had an average oxidative peak current in FC of  $+9.63 \pm 1.09 \mu\text{A}$ , after SAM formation this dropped to  $+6.85 \pm 0.68 \mu\text{A}$ . The reduction peaks dropped from  $-7.52 \pm 1.03$  to  $-4.99 \pm 1.10 \mu\text{A}$  after film formation. By assuming the diffusion coefficient of both ferricyanide and ferrocyanide to be  $7 \times 10^{-6} \text{ cm}^2 \text{ s}^{-1}$  and the room temperature to be 293 Kelvin the electroactive surface area can be obtained from the Randles–Sevcik equation (Equation (2))<sup>[36]</sup>

$$i_l = 0.4463nFAc \left( \frac{nFvD}{RT} \right)^{\frac{1}{2}} \quad (2)$$

where  $i_l$  is the limiting current,  $n$  is the number of electrons being transferred,  $F$  is Faraday constant,  $A$  is the electrochemically active surface area,  $c$  is the concentration of the redox agent in the bulk solution,  $v$  is the scan rate of the CV,  $D$  is the diffusion coefficient of the redox agent,  $R$  is the universal gas constant, and  $T$  is the temperature in Kelvin. This analysis is valid because the peak current scales linearly with the square root of the scan rate, see Figure S7 in the Supporting Information. This analysis shows that from the oxidative peak currents the bare electrode has an active surface area of  $7.75 \text{ mm}^2$  that drops to  $5.51 \text{ mm}^2$  after MCH SAM formation, a drop of 28.9%. The reductive peak currents correlate to an area of  $6.06 \text{ mm}^2$  for the bare yarn which dropped to  $4.02 \text{ mm}^2$  after SAM formation, a drop of 33.6%. This analysis was also performed using literature values for the diffusion coefficient of MB and RHC and the results are included in Table S2 (Supporting Information).<sup>[37,38]</sup> If the multifilament Au yarn was treated as a solid cylinder with a diameter of  $250 \mu\text{m}$  and a length of 13 mm, its geometric surface area would be  $10.2 \text{ mm}^2$ . Alternatively, if each filament is treated as a cylinder with a diameter of  $20 \mu\text{m}$ , given that there are 72 filaments in the yarn, the maximum area that could be exposed to solution would be  $58.81 \text{ mm}^2$ . It is therefore satisfying that the active surface area lies within the same order of magnitude as these values. It is important to note that the geometrical areas approached could never be reached as contacts between filaments cannot wet and be electrochemically active. Also, because the yarns are used as provided they may be dirty or scratched which would account for the measured electrochemically active surface areas being lower than the geometric areas. It is also satisfying that for all values calculated for each redox agent the decrease in accessible electrode surface is about a third of the total surface area. This is in good agreement with the literature<sup>[5,39]</sup> and shows that these yarns form equally good SAM coverage to commercial disc electrodes. The ability to form SAMs with as good a coverage on these yarns off the shelf as good as those on cleaned commercial electrodes is encouraging. Typically electrodes need to be cleaned by mechanical polishing, chemical cleaning (usually piranha) and electrochemical cycling prior to functionalization in order to get good reproducible SAM coverage.<sup>[40,41]</sup> The ability to use these Au yarns without any of this treatment and get the reproducibility and coverage observed

here is a key finding and major advantage of these yarns which makes them ideally suited for future biosensor development. The reasons for these yarns being so good are currently under investigation but it is thought that the multiple filaments may in a way polish each other as they rub against one another during handling. While this may in theory remove any SAM from the filaments it is likely that these SAMs that have been physically detached would be likely to rebind to neighboring filaments and would not be lost from the multifilament as a whole.

The CNT yarns were first characterized by measuring their CVs using the same redox agents in PBS as for the Au yarn, see Figure S8 in the Supporting Information for CVs in FC, and their ability to be functionalized was determined by electrochemically binding 6-aminohexan-1-ol to the CNT yarns using the method developed by Deinhammer and Porter.<sup>[28]</sup> The CNT yarns did not perform as well as the Au yarns so were not taken forward in this study.

Weaving the yarns into a series of different designs allows us to create devices capable of performing different microfluidic functions. In order to better illustrate how these devices are being woven together we have developed a component model diagram, shown next to schematic illustrations and photos of the functioning devices in **Figure 3**. Figure 3A acts as a legend for the component model diagrams in Figure 3B–F and shows how weaving the yarns in different fashions allows for the fabrication of capillary force driven microfluidic fluid transport and mixing devices using nonfluidic, fluidic, and electrofluidic threads. We use the term electrofluidic because the conductive yarn also transports fluids due to capillary actions between the filaments. The devices in Figure 3 not only show that the woven designs are capable of fluid transport and mixing but also that the yarns exhibit true microfluidic behavior. As seen in Figure 3F where yarns running parallel and in contact with each other can keep dyes from mixing due to only having laminar flow. Left over time, see Video S1 in the Supporting Information, these dyes mix through diffusion at the interface between the two yarns. This is indicative of low Reynolds numbers characteristic of microfluidics, i.e., predominantly laminar rather than turbulent flow. If we assume that the dyes in Figure 3 have the same properties as water and that the characteristic linear dimension of the yarns is the diameter of the largest Coolmax yarns (a diameter of 896  $\mu\text{m}$ ) then we can calculate the Reynolds numbers of the Coolmax yarns from the wicking tests in Figure 1 and Equation (3)

$$R_e = \rho u L / \mu \quad (3)$$

where  $R_e$  is the Reynolds number,  $\rho$  is the fluid density,  $u$  is the velocity of the fluid,  $L$  is the characteristic linear dimension (taken as the diameter of the multifilament yarn), and  $\mu$  is the dynamic viscosity of the fluid. Accepting that several assumptions have had to be made the yarns wicking 70 mm in 120 s would have Reynolds numbers of  $<50$ . This is far below the accepted threshold for turbulent flow (200) so, even allowing for the error in our assumptions we can say with some confidence that the Coolmax filaments are all going to exhibit predominantly laminar flow, which is supported by the data in Figure 3F.

We performed simple tests adding dyes to the different inlets to demonstrate the microfluidic behavior of the different device designs. The device in Figure 3B illustrates how multiple separate channels can be woven. The device in Figure 3C shows both how parallel yarns can be joined to form larger channels and how fluidic barriers can prevent the flow from yarns across junctions. Figure 3D illustrates how several yarns in the weft direction can connect at junctions to create a fluidic separator.

Figure 3E shows a fluidic mixer in which two different flows enter from each side of a weft yarn, mix in a single junction and enter a common warp yarn as mixed fluids. As seen in Figure 3F, parallel yarn in fluidic contact mix only through diffusion at the interface between the two yarns. The videos included in the supplementary information show the devices in use. One of the key highlights of the Coolmax yarns is the speed with which they wick the solutions, as shown in Figure 1A. Typical methods of microfluidic fabrication usually require external pumps to flow over such distances and rarely achieve the speed of fluid transport observed here.<sup>[3,23]</sup> The ability to wick such small sample volumes so quickly by capillary forces alone is a key advantage to using textiles over other microfluidic architectures.

In order to make functional sensors in the woven devices we need to incorporate the electrofluidic yarns into the weaves to act as counter, reference, and working electrodes. **Figure 4A** shows the component model diagram, schematic illustration and photograph of this device. In the devices shown we use the Au yarn to make an Au/Au/Au three electrode system using single Au yarns to act as working and pseudoreference electrodes and two Au yarns as a counter electrode. These experiments were originally conducted using Ag yarn as a pseudoreference electrode, however, this was found not to be suitable for the glucose sensing experiments below as silver dissolves in the presence of  $\text{H}_2\text{O}_2$ . For other sensing systems the Ag yarn would be appropriate and methods to convert it to a formal Ag/AgCl reference electrode suitable for incorporation in these woven devices is currently under investigation.

A typical cyclic voltammogram of the Au/Au/Au set up in PBS with  $1 \times 10^{-3}$  M FC with all the yarns dipped in solution is included in Figure 4B. In Figure 4C three yarns were woven into separate devices (photographed in 4A), the wicking channel was wet with 10  $\mu\text{L}$  of  $1 \times 10^{-3}$  M FC in PBS and CVs recorded. Figure 4B,C are direct comparisons of the Au threads in and out of a weave to determine what effect weaving has on the observed electrochemistry. The oxidation and reduction peaks for all threads in solution and in the weave have been analyzed and their data is summarized in Table S2 (Supporting Information). The first difference when going into a weave is that a decrease in peak current is observed. This could be down to several factors, such as damaging and/or fouling of the yarns as they are handled during the weaving process. If so then large scale manufacturing of the woven devices would make such damaging more reproducible and even conceptually reduce any fouling introduced when weaving by hand. Another possible explanation for the reduction in peak current is the change in the wetting of the yarns. In solution the yarn is completely surrounded by solvated ions and redox agents are free to diffuse in and out of the yarns with ease. In the woven devices the solution has to wick along the Coolmax and then through the

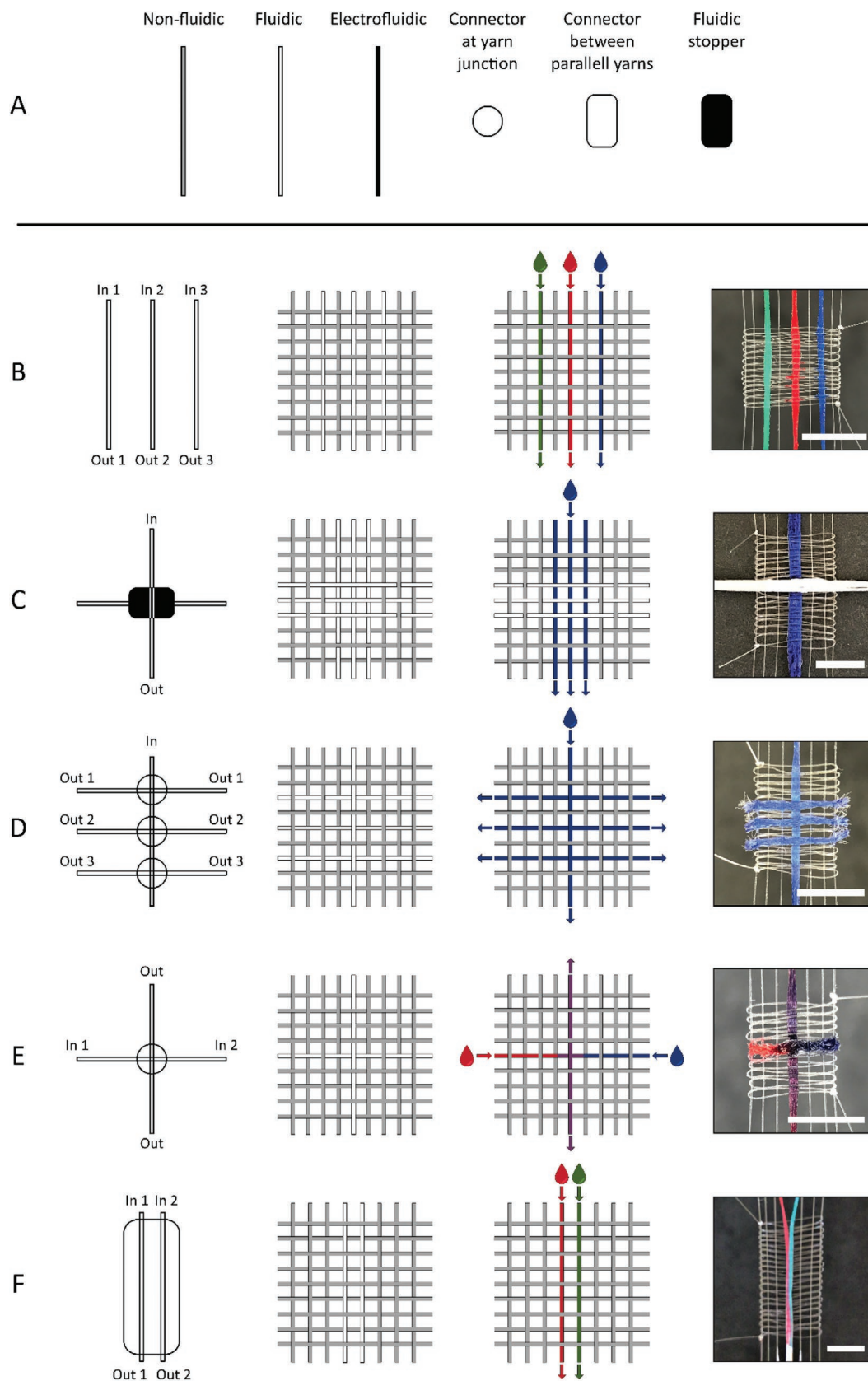


**Figure 3.** Component model diagram, schematic illustrations and photos of woven devices for various integrated microfluidic functions in weaves. Scale bars show 5 mm.

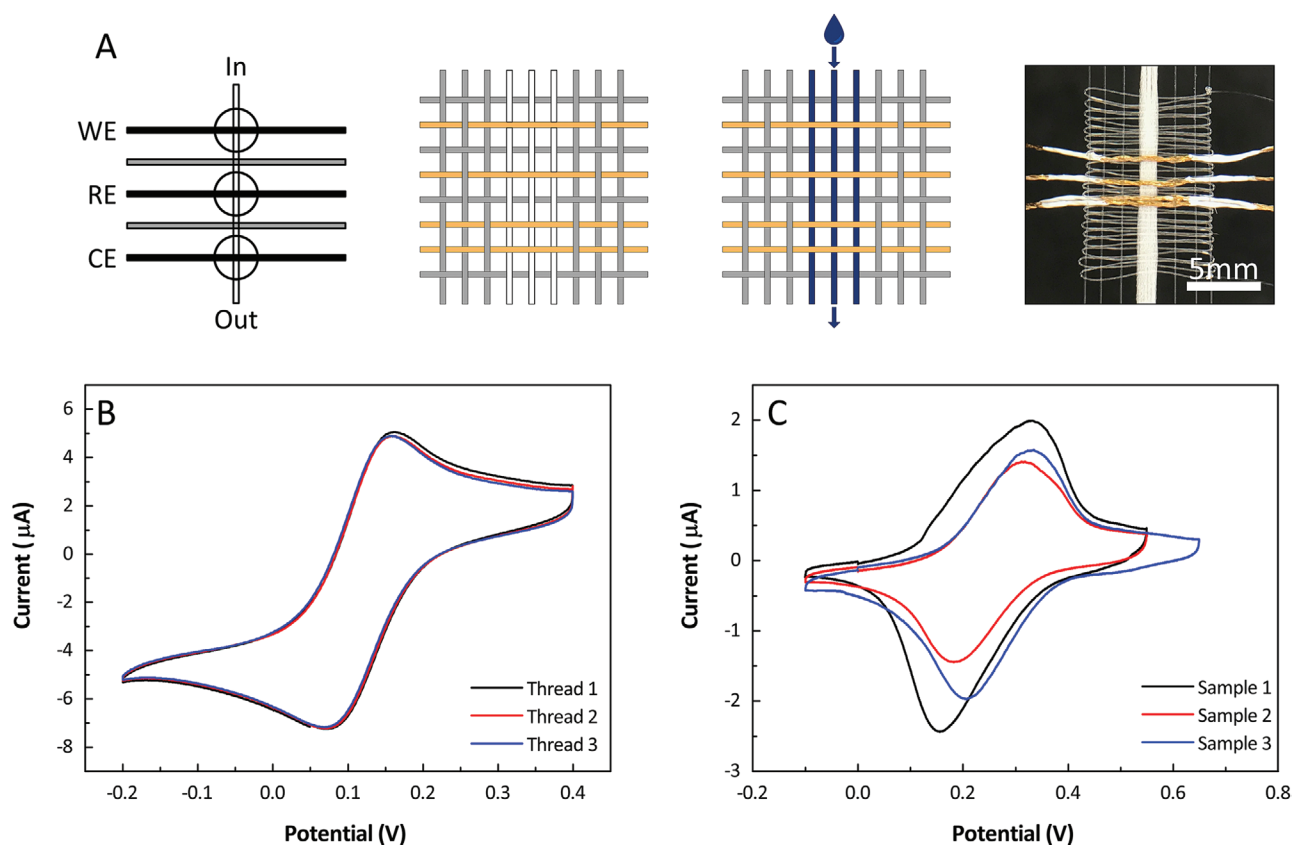


**Figure 4.** A) Model diagram, schematic illustration and photo of a woven electrochemical three electrode system together with B) CVs for three repeats in solution and C) three repeats in a weave.

conductive yarns themselves. In the woven system the core of the multifilament is wet whereas in solution the core and exterior of the yarn are in direct contact with solution. We would therefore expect a smaller current from the yarns in a weave. There is also a difference in peak shape between Figure 4B and Figure 4C, the woven devices have sharper peaks and the yarns in solution have more wave like peaks. This is attributed to the different diffusional regimes in the different systems. In the woven yarns the solution is wicking along the yarn and confined to the core of the multifilament so the observed electrochemistry is similar to thin layer electrochemical set ups. By this it is meant that finite diffusional regimes are observed in the weave but semi-infinite linear regimes are observed in solution. It should be noted that a part of the electrofluidic Au yarn is in constant contact with the wicking Coolmax yarn so will have a flow of redox agent and fresh electrolyte coming to it that may be different to the edges of the yarn. Also Marangoni effects may in time concentrate the redox agent and electrolyte at the end of the conductive yarn (next to the nail varnish barriers, see Figure S6A in the Supporting Information). It is therefore likely that the response over the whole yarn is not uniform.

At first glance it appears that there is a greater variation between the yarns when woven than when in solution (when observing the variation in peak currents between Figure 4B and Figure 4C). The average oxidative and reductive currents

in solution are  $5.83 \pm 0.10$  and  $5.04 \pm 0.24$   $\mu\text{A}$ , respectively. In the weave the corresponding values are  $1.40 \pm 0.23$  and  $1.64 \pm 0.43$   $\mu\text{A}$ , respectively. While in the woven devices the proportional variation is much larger than in solution, the absolute values of the deviations seen in Figure 4B,C are the same order of magnitude. Therefore, the difference in these variations could be the result of random uncontrollable experimental errors such as buffer preparation. Randles-Sevcik analysis of the yarns in a weave was not conducted as it assumes semi-infinite linear diffusion,<sup>[34]</sup> which is not observed in these systems.

Having established the best choice of yarns, characterized them and developed a woven device capable of electrochemical measurements, a proof of concept device capable of detecting glucose in artificial human sweat was developed. In order to create a functional glucose sensor on the working electrode yarn, a MCHA SAM was formed on the yarn overnight prior to weaving. This was then activated by EDC and NHS to allow the covalent coupling of GOx to the yarn via standard carbodiimide coupling, see materials and methods for details. Once bound to the electrode surface the active GOx oxidizes glucose to gluconolactone, creating  $\text{H}_2\text{O}_2$  as a by-product which can be detected electrochemically, see Figure 5A. In this process the GOx is itself reduced and cannot oxidize any more glucose without being converted back to its oxidized form. By adding a redox agent (RHC) to the solution it is possible to regenerate the oxidized form of

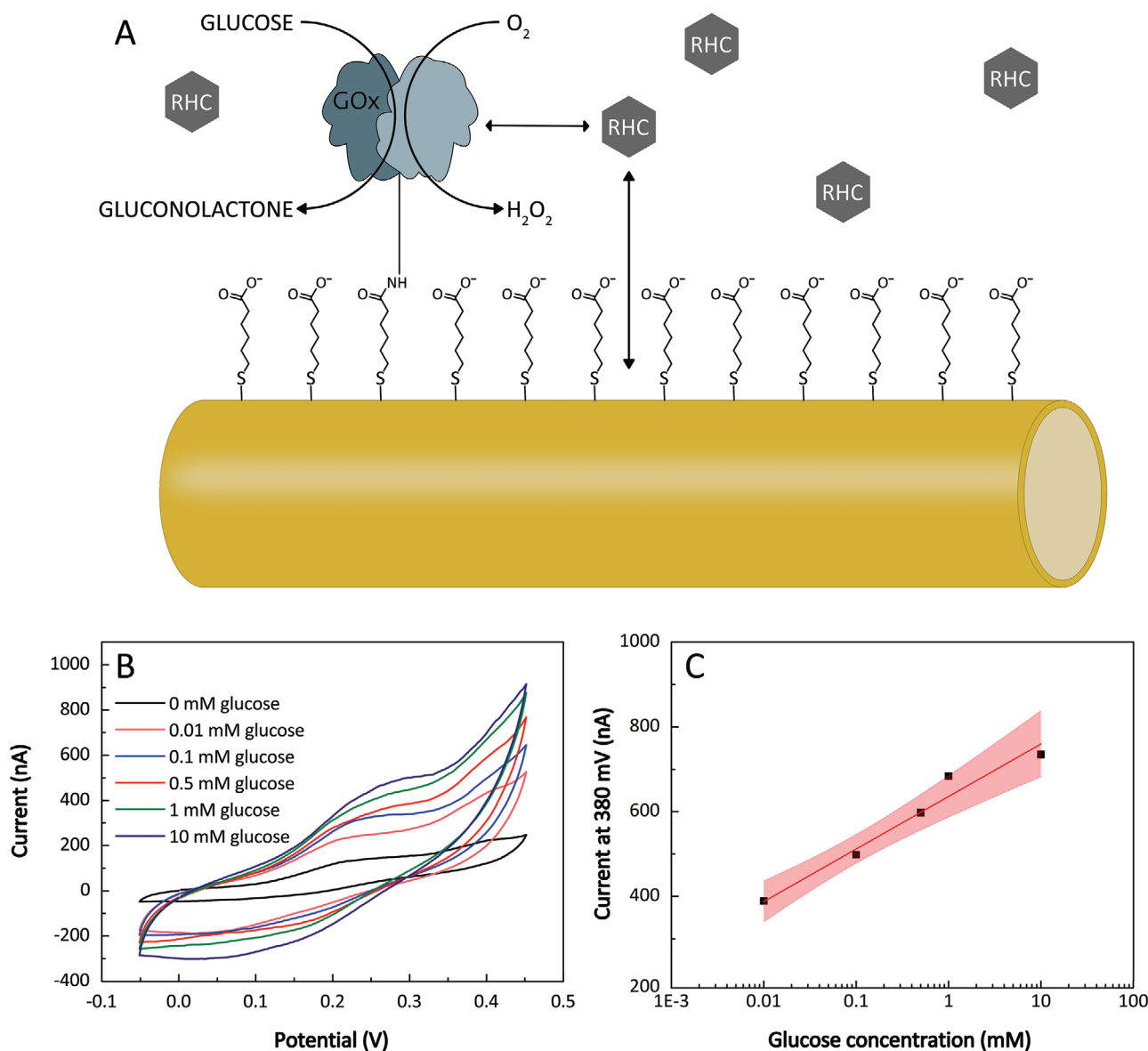


**Figure 5.** A) Schematic illustration of glucose oxidase bound to a gold filament, the reaction with glucose in solution and reducing action of ruthenium hexamine chloride (RHC) in solution. B) Cyclic voltammograms (CVs) showing the change in response with increasing glucose concentration in artificial human sweat from one of the typical devices tested. CVs were recorded at  $10 \text{ mV s}^{-1}$ . C) The log dose response curve for increasing glucose concentrations,  $n = 7$ , with a 95% confidence interval shown in red.

GOx and realize a continuous glucose sensor.<sup>[42,43]</sup> A schematic illustration of the mode of operation showing the GOx bound to MCHA and the regeneration of the glucose oxidase by RHC is provided in Figure 5A. The scan rate and potential window are important and were optimized here to be  $10 \text{ mV s}^{-1}$  and  $-0.05$  to  $+0.45 \text{ V}$  versus the pseudo reference electrode, respectively. This needed to be long and slow enough to ensure the complete regeneration of the GOx by the RHC, which led to a more stable  $\text{H}_2\text{O}_2$  peak across successive scans, while being fast enough to be able to cycle several times before the device would dry out (which took  $\approx 15 \text{ min}$  when  $10 \mu\text{L}$  of sweat was added). The voltage window also needed to be large enough to find all the relevant peaks while

avoiding the chloride reduction and oxygen adsorption peaks which may damage the SAM.

Given that this is an all textile woven device it can in theory be made on an industrial scale and used as a wearable diagnostic. It therefore makes logical sense to develop a sensor capable of detecting analytes in human sweat. Studies have shown the feasibility of measuring glucose levels in sweat and how these correlate to blood glucose levels.<sup>[44]</sup> The clinically relevant glucose levels in human sweat are between  $0.277 \times 10^{-3}$  and  $1.11 \times 10^{-3} \text{ M}$ ,<sup>[45]</sup> we therefore tested our devices in artificial human sweat spiked with increasing concentration of glucose between  $0.01 \times 10^{-3}$  and  $10 \times 10^{-3} \text{ M}$ . It is satisfying that our devices have a linear response across the range tested,

greater than the clinically relevant range, and a limit of detection of  $635 \pm 15 \times 10^{-9}$  M, see Figure 5C. Two recent reviews on the topic of wearable sweat based glucose detection show that a wide variety of devices have been demonstrated as suitable for this purpose.<sup>[46,47]</sup> However, in these reviews there is no mention of using textiles, which have obvious advantages when it comes to wearable devices and sweat based diagnostics as they can be incorporated into clothing. The woven devices reported here also have a wider dynamic range and lower limit of detection that is normally reported for glucose detection in sweat, with the added advantage of being textile based so can be easily and readily incorporated into clothing for wearable sensors. These low limits of detection and wide dynamic ranges make these devices suitable for the detection of less concentrated biomarkers in sweat: such as proteins, hormones and drugs.

The long term stability of these devices is not currently known but under current investigation. The current set up does not lend itself to sensor stability measurements due to the fact that the devices presented here are static, i.e., operate without sweat flowing over them. One of the main causes of GOx degradation is the oxidation of methionine by  $H_2O_2$ . In a flowing system the  $H_2O_2$  created by the oxidation of glucose by GOx will be carried away from the sensor surface, as such without flow there will be a higher rate of GOx degradation than in a flowing device. As such it is merely noted in this work that the devices were all tested within 48 h of fabrication and that similar in vivo sensors that use GOx have been shown to be stable for days<sup>[48]</sup> and we anticipate these devices to exhibit similar stabilities.

This approach offers various advantages over the current glucose monitoring systems for diabetes as no blood sampling is required. This is a continuous measurement being taken in real time so could theoretically be linked to an insulin release device to realize a wearable “smart” system that keeps a patient’s glucose levels constant, which is better for patient outcomes than the current peaks and troughs in blood glucose levels which result from self-testing.<sup>[49]</sup> The stability of GOx means that, in theory, these devices should remain active for months when stored under the correct conditions;<sup>[48]</sup> albeit with some variation from the underlying MCHA SAM. Ongoing work to incorporate this sensor with a wearable potentiostat will allow for the proper determination of the stability of the sensor when worn, as the stability might be affected by body temperature and sweat rate.

As well as diabetes monitoring, noninvasive glucose detection can also be used for sports activity monitoring. Sweat contains an abundance of biomarkers<sup>[17,45,50]</sup> and it is hoped that this proof of principle device will show that woven diagnostic devices fabricated with mass produced yarns will inspire the development of wearable sensors for other biomarkers.

To the best of the authors’ knowledge this is the first time that a fully woven textile device made from off-the-shelf yarns available on an industrial scale has been made. The innate ability of these yarns to be woven together to make functional devices without the need for cleaning or complex processing should not be understated. The ability to get good electrochemical responses and a SAM coverage as good as cleaned commercial Au electrodes on the Au multifilament threads as they

arrive, without any cleaning, is one of the major findings of this work. This performance coupled with their low cost makes the multifilament threads ideally suited for mass produced electrochemical diagnostics fabrication as well as lab based research.

Coolmax yarns have been used for many years in the sportswear industry and were specifically designed to wick sweat. Here we report for the first time the use of these yarns in  $\mu$ TAS. We demonstrate the ability of these yarns to perform basic microfluidic functions and estimate their Reynolds numbers as well as measuring their retention of example biomolecules across a wicked length. Such analysis for other sensing media such as blood and urine are the topic of further investigation and show promise for the use in smart bandages and diapers.

As a proof of principle the coolmax and multifilament Au yarns have been woven into a wearable device capable of detecting glucose in artificial human sweat in the clinically relevant range. This offers obvious advantages for diabetes diagnostics and sportswear manufacturers where a noninvasive, continuous and wearable glucose monitor would be advantageous. While wearable sweat based diagnostics is not in itself novel, it has been reported here to show the feasibility of making operational sweat based diagnostics from these yarns. It is pleasing that it does so over a clinically relevant range.

Further work is required to miniaturize the electrical components to achieve a truly wearable device, as well as optimization to operate at on-body temperatures. The development of a formal Ag/AgCl reference electrode on the Ag yarn would allow the development of potential dependent sensing modalities, such as electrochemical impedance spectroscopy, and as such is an active area of research within the Hamedi group. Given the abundance of biomarkers within sweat, ongoing research will focus on developing this platform to detect other analytes of interest as well as optimization to work in other sample solutions such as blood and urine.

## Experimental Section

**Materials:** Table S1 (Supporting Information) summarizes all the yarns used in this study, where they have been purchased from and their important physical properties. Phosphate-buffered saline (PBS), ruthenium hexamine chloride (RHC), potassium ferricyanide (FC), methylene blue (MB), glucose oxidase (GOx), glucose, 6-mercaptohexan-1-ol (MCH), 6-mercaptohexanoic acid (MCHA), *N*-(3-dimethylaminopropyl)-*N*’-ethylenecarbodiimide (EDC), and *N*-hydroxysuccinimide (NHS) were purchased from Sigma Aldrich (Sweden). Synthetic ssDNA for nitrogen concentration analysis was bought from Eurofins genomics and the artificial sweat from VWR (Sweden). Red and green food coloring for demonstration of our fluidic devices were produced by Dr. Oetker (Purchased from a supermarket in Sweden). Commercial Ag/AgCl reference electrodes were purchased from VWR (VWR, Sweden)

**SEM Characterization of Yarns:** Characterization of the structures, surfaces and cross-sections of the different yarns was done using a Hitachi Tabletop SEM TM-1000 (Japan) with BSE detector and W filament in charge-up reduction mode.

**Wicking Tests:** The wicking behavior for the three different Coolmax yarns was measured using a simple test set up for vertical wicking. The yarns were cut to five samples of 35 cm length. Weights of  $4.78 \pm 0.04$  g were attached to one end of the yarns while the other was attached to a stand, placing the yarns in a vertical hanging position with tension



introduced by the weights. Two centimeters of the yarn samples were immersed in ultrapure (Milli-Q) water containing  $1 \text{ g L}^{-1}$  methylene blue and allowed to wick for five minutes. A ruler was attached behind the wicking yarn, making it possible to measure how far the dye wicked up the yarn. A schematic illustration of the set-up has been included in Figure S1 (Supporting Information). Video footage was recorded on an iPhone 7+ (Apple Inc., Sweden) and was analyzed by collecting data points for the wicking distance every 10 s. Unless otherwise stated, all data in this article was plotted and analyzed in Origin 9.1 (OriginLab).

**Determining Analyte Distribution Over a Wicking Yarn:** To characterize if any concentration losses were done over wicking distance in the yarn BSA, RHC, and synthetic 17 mer ssDNA were used in concentrations of  $35 \text{ g L}^{-1}$ ,  $5 \times 10^{-3} \text{ M}$ , and  $100 \times 10^{-6} \text{ M}$ , respectively. Three yarn cuts of the Coolmax yarn dtex78/f48/2 for each solution (making a total of nine samples) were placed horizontally, in tension and hanging freely in the air to prevent that wicking between the yarn and substrate would occur. At one end of the yarns, a fluidic barrier was created using nail varnish to stop the solutions from wicking in that direction.  $5 \mu\text{L}$  of solution was added to each yarn and allowed to wick and dry for 30 min. After drying, the yarns were cut into 1 cm fragments and the nitrogen content was measured in each using an ANTEK Multitek Nitrogen Analyzer (PAC Multitek, Sweden). This equipment works by incinerating the samples at  $1050 \text{ }^\circ\text{C}$  and 3 bar of Oxygen (Strandmöllen, Sweden) and measures the amount of N present using pyro-chemiluminescence, with a limit of detection quoted from the manufacturer of 15 ppb.

**Cyclic Voltammetry of Conductive Yarns:** All electrochemical measurements were performed on an Autolab PGSTAT204N with MUX 16 module (Metrohm Autolab, Sweden) using the accompanying NOVA 1.11 software package. Characterization of the Au coated yarn as working electrode in an electrochemical three electrode set up was performed in solutions of PBS containing  $1 \times 10^{-3} \text{ M}$  of FC, RHC or MB. CVs were recorded for five samples at  $30 \text{ mV s}^{-1}$  versus a Pt counter electrode and an Ag/AgCl reference electrode.

**MCH SAM Formation on Au Yarns:** Five Au coated yarns were functionalized overnight in ethanol with  $1 \times 10^{-3} \text{ M}$  MCH followed by rinsing in ethanol and PBS. CVs were recorded at  $30 \text{ mV s}^{-1}$  versus a Pt counter electrode and an Ag/AgCl reference electrode for comparison with the results of bare electrodes and calculation of electrochemical surface area.

**6-Aminohexanol Coupling to CNT Yarns:** The procedure for these experiments was previously published by Deinhammer et al.<sup>[28]</sup> Briefly, electrodeposition was done in ethanol with  $100 \times 10^{-3} \text{ M}$   $\text{NaClO}_4$  at  $5 \text{ mV s}^{-1}$  versus a Pt counter electrode and Pt pseudo reference electrode. CVs of the bare CNT yarns were performed under the same conditions as the Au yarns.

**Weaving and Testing Capillary Force Driven Microfluidic Devices:** Weaving was carried out using a simple hand loom, see Figure S2 in the Supporting Information (purchased from Slöjd-Detaljer). All devices throughout this article have been made using a plain weave pattern meaning that the weft yarns (yarns in x-direction in Figure 3) crosses the warp yarns (yarns in y-direction in Figure 3) by going above and below them alternatively at each junction. Every additional weft yarn crosses the warp yarns in the opposite way of the previous one, creating a simple crisscross pattern. In the devices where several yarns were bundled in parallel to create wider fluidic channels, floats were introduced to the weave patterns. Floats occur when a warp or weft yarn skip interfering with some of the opposing yarns and instead goes above or below them all. To demonstrate the woven capillary force driven microfluidic devices, red (carmin dye) and green (lutein and brilliant blue dyes) food coloring as well as methylene blue dye were used. All woven capillary force driven microfluidic devices were made using the PA monofilament as a hydrophobic network with integrated Coolmax dtex78/f48/2 as fluidic channels. Specific Coolmax yarn was chosen to work with over the other two because it wicks fast but is thinner than the other two.

**Woven Three Electrode Device Fabrication and Testing:** To realize a woven device with an integrated three electrode system, fluidic barriers were patterned on the conductive yarns. Within a woven network of

monofilament yarns, Au yarn was integrated as working electrode, Ag yarn as pseudoreference electrode, and two Au yarns as counter electrode in the weft as well as a wicking channel of Coolmax dtex78/f48/2 in the warp.  $10 \mu\text{L}$  of  $1 \times 10^{-3} \text{ M}$  FC in PBS was added to the channel and allowed to wick across the device before CVs were recorded at  $30 \text{ mV s}^{-1}$ .

**Functionalizing Au Yarns for Glucose Sensing:** Functionalization was done overnight in a solution of  $1 \times 10^{-3} \text{ M}$  MCHA in ethanol (25 mL total volume). After rinsing with ethanol and PBS, EDC-NHS coupling was done in 50 mL PBS with  $4 \times 10^{-3} \text{ M}$  EDC and  $1 \times 10^{-3} \text{ M}$  NHS for 10 min. Further,  $0.1 \text{ mg mL}^{-1}$  GOx was added to the solution for another 10 min. Lastly, the electrodes were rinsed and stored in PBS, pH 7.4.

**Detecting Glucose in Artificial Human Sweat:** The functionalized yarns were integrated in a woven network of nonfluidic monofilament yarn and fluidic Coolmax dtex78/f48/2 as well as Au yarn counter and Au yarn pseudoreference electrodes. Solutions of  $5 \times 10^{-3} \text{ M}$  RHC in artificial sweat (pH 6.59) with glucose concentrations ranging from  $0.01 \times 10^{-3}$  to  $10 \times 10^{-3} \text{ M}$  were added to the wicking channel ( $10 \mu\text{L}$ ) and CVs were recorded at  $10 \text{ mV s}^{-1}$  until the device dried out after roughly 15 min.

## Supporting Information

Supporting Information is available from the Wiley Online Library or from the author.

## Acknowledgements

I.Ö.M. and A.P. contributed equally to this work. The authors thank Contifibre for providing Coolmax yarn, and Swicofil for guidance and discussions on the metal plasma coated yarns. The authors also acknowledge the Knut and Alice Wallenberg Foundation and the European Research Council (Grant 715268) for funding.

## Conflict of Interest

The authors declare no conflict of interest.

## Keywords

electroanalytical devices, e-textile, micro total analysis, microfluidics

Received: April 27, 2020

Revised: June 30, 2020

Published online:

- [1] M. Zarei, *Biosens. Bioelectron.* **2017**, *98*, 494.
- [2] S. K. Vashist, *Biosensors* **2017**, *7*, 62.
- [3] L. Zhang, B. Z. Ding, Q. H. Chen, Q. Feng, L. Lin, J. S. Sun, *TrAc, Trends Anal. Chem.* **2017**, *94*, 106.
- [4] A. Piper, B. Alston, D. Adams, A. R. Mount, *Faraday Discuss.* **2018**, *210*, 201.
- [5] A. Piper, Ph.D. Thesis, University of Edinburgh, **2017**.
- [6] D. E. Presnov, I. V. Bozhev, A. V. Miakonkikh, S. G. Simakin, A. S. Trifonov, V. A. Krupenin, *J. Appl. Phys.* **2018**, *123*, 054503.
- [7] N. Couniot, T. Vanzieleghem, J. Rasson, N. Van Overstraeten-Schlogel, O. Poncelet, J. Mahillon, L. A. Francis, D. Flandre, *Biosens. Bioelectron.* **2015**, *67*, 154.
- [8] P. Quan Li, A. Piper, I. Schmuesser, A. R. Mount, D. K. Corrigan, *Analyst* **2017**, *142*, 1946.

- [9] R. B. Channon, Y. Y. Yang, K. M. Feibelman, B. J. Geiss, D. S. Dandy, C. S. Henry, *Anal. Chem.* **2018**, *90*, 7777.
- [10] S. Rengaraj, A. Cruz-Izquierdo, J. L. Scott, M. Di Lorenzo, *Sens. Actuators, B* **2018**, *265*, 50.
- [11] I. Kleps, A. Angelescu, R. Vasilco, D. Dascalu, *Biomed. Microdevices* **2001**, *3*, 29.
- [12] E. Carrilho, A. W. Martinez, G. M. Whitesides, *Anal. Chem.* **2009**, *81*, 7091.
- [13] A. Nilghaz, D. R. Ballerini, W. Shen, *Biomicrofluidics* **2013**, *7*, 51501.
- [14] A. Yang, Y. Li, C. Yang, Y. Fu, N. Wang, L. Li, F. Yan, *Adv. Mater.* **2018**, *30*, e1800051.
- [15] T. Choudhary, G. P. Rajamanickam, D. Dendukuri, *Lab Chip* **2015**, *15*, 2064.
- [16] H. Derakhshandeh, S. S. Kashaf, F. Aghabaglou, I. O. Ghanavati, A. Tamayol, *Trends Biotechnol.* **2018**, *36*, 1259.
- [17] G. Matzeu, L. Florea, D. Diamond, *Sens. Actuators, B* **2015**, *211*, 403.
- [18] W. Gao, S. Emaminejad, H. Y. Y. Nyein, S. Challa, K. V. Chen, A. Peck, H. M. Fahad, H. Ota, H. Shiraki, D. Kiriya, D. H. Lien, G. A. Brooks, R. W. Davis, A. Javey, *Nature* **2016**, *529*, 509.
- [19] H. Y. Y. Nyein, L. C. Tai, Q. P. Ngo, M. H. Chao, G. B. Zhang, W. Gao, M. Bariya, J. Bullock, H. Kim, H. M. Fahad, A. Javey, *ACS Sens.* **2018**, *3*, 944.
- [20] M. Reches, K. A. Mirica, R. Dasgupta, M. D. Dickey, M. J. Butte, G. M. Whitesides, *ACS Appl. Mater. Interfaces* **2010**, *2*, 1722.
- [21] X. Li, J. Tian, W. Shen, *ACS Appl. Mater. Interfaces* **2010**, *2*, 1.
- [22] A. Nilghaz, S. Bagherbaigi, C. L. Lam, S. M. Mousavi, E. P. Córcoles, D. H. B. Wicaksono, *Microfluid. Nanofluid.* **2015**, *19*, 317.
- [23] P. Mostafalu, M. Akbari, K. A. Alberti, Q. Xu, A. Khademhosseini, S. R. Sonkusale, *Microsyst. Nanoeng.* **2016**, *2*, 16039.
- [24] P. Bhandari, T. Narahari, D. Dendukuri, *Lab Chip* **2011**, *11*, 2493.
- [25] A. Lund, S. Darabi, S. Hultmark, J. D. Ryan, B. Andersson, A. Ström, C. Müller, *Adv. Mater. Technol.* **2018**, *3*, 1800251.
- [26] X. Liu, P. B. Lillehoj, *Lab Chip* **2016**, *16*, 2093.
- [27] T. Choudhary, G. P. Rajamanickam, D. Dendukuri, *Lab Chip* **2015**, *15*, 2064.
- [28] R. S. Deinhammer, M. Ho, J. W. Andereg, M. D. Porter, *Langmuir* **1994**, *10*, 1306.
- [29] D. Spencer, in *Knitting Technology*, Elsevier Ltd, Amsterdam **1983**, Ch. 1, p. 1.
- [30] R. Safavieh, G. Z. Zhou, D. Juncker, *Lab Chip* **2011**, *11*, 2618.
- [31] E. Fu, B. Lutz, P. Kauffman, P. Yager, *Lab Chip* **2010**, *10*, 918.
- [32] A. Nilghaz, D. H. Wicaksono, D. Gustiono, F. A. Abdul Majid, E. Supriyanto, M. R. Abdul Kadir, *Lab Chip* **2012**, *12*, 209.
- [33] N. Wang, A. Zha, J. Wang, *Fibers Polym.* **2008**, *9*, 97.
- [34] A. J. Bard, L. R. Faulkner, *Electrochemical methods: fundamentals and applications*, Wiley, New York **1980**.
- [35] E. Gileadi, *Physical Electrochemistry-Fundamentals, Techniques and Applications*, Wiley-VCH Verlag GmbH & Co. KGaA, Weinheim **2015**.
- [36] S. J. Konopka, B. McDuffie, *Anal. Chem.* **1970**, *42*, 1741.
- [37] D. G. Leaist, *Can. J. Chem.* **1988**, *66*, 2452.
- [38] J. M. Moldenhauer, M. Meier, W. Paul David, *J. Electrochem. Soc.* **2016**, *163*, H3135.
- [39] T. Wink, S. J. vanZuilen, A. Bult, W. P. vanBennekom, *Analyst* **1997**, *122*, R43.
- [40] L. M. Fischer, M. Tenje, A. R. Heiskanen, N. Masuda, J. Castillo, A. Bentien, J. Emneus, M. H. Jakobsen, A. Boisen, *Microelectron. Eng.* **2009**, *86*, 1282.
- [41] J. M. Campina, A. Martins, F. Silva, *Electrochim. Acta* **2008**, *53*, 7681.
- [42] E.-H. Yoo, S.-Y. Lee, *Sensors* **2010**, *10*, 4558.
- [43] A. Heller, B. Feldman, *Chem. Rev.* **2008**, *108*, 2482.
- [44] J. Moyer, D. Wilson, I. Finkelshtein, B. Wong, R. Potts, *Diabetes Technol. Ther.* **2012**, *14*, 398.
- [45] O. Mickelsen, A. Keys, *J. Biol. Chem.* **1943**, *149*, 479.
- [46] M. C. Brothers, M. DeBrosse, C. C. Grigsby, R. R. Naik, S. M. Hussain, J. Heikenfeld, S. S. Kim, *Acc. Chem. Res.* **2019**, *52*, 297.
- [47] H. Lee, Y. J. Hong, S. Baik, T. Hyeon, D. H. Kim, *Adv. Healthcare Mater.* **2018**, *7*, e1701150.
- [48] M. Chung, G. Fortunato, N. Radacsi, *J. R. Soc. Interface* **2019**, *16*, 20190217.
- [49] N. Brasier, J. Eckstein, *Digital Biomarker* **2019**, *3*, 155.
- [50] B. A. Katchman, M. L. Zhu, J. B. Christen, K. S. Anderson, *Proteom. Clin. Appl.* **2018**, *12*, e1800010.